Scripta Materialia 162 (2019) 251–255

Contents lists available at ScienceDirect

Scripta Materialia

journal homepage: www.elsevier.com/locate/scriptamat

Comparison of the grain growth behavior and defect structures of flash sintered ZnO with and without controlled current ramp

Xin Li Phuah [a], Han Wang [a], Harry Charalambous [b], Shikhar Krishn Jha [b], Thomas Tsakalakos [b], Xinghang Zhang [a], Haiyan Wang [a,c,*]

[a] School of Materials Engineering, Purdue University, West Lafayette, IN 47907, USA
[b] Department of Materials Science and Engineering, Rutgers University, New Brunswick, NJ 08901, USA
[c] School of Electrical and Computer Engineering, Purdue University, West Lafayette, IN 47907, USA

ARTICLE INFO

Article history:
Received 22 July 2018
Received in revised form 26 October 2018
Accepted 3 November 2018
Available online xxxx

Keywords:
Flash sintering
Controlled current ramp
ZnO
Microstructure
TEM

ABSTRACT

During the flash sintering of ceramics, rapid densification occurs during the non-linear increase in current. To investigate the effect of an abrupt increase in current, a detailed microstructure characterization of flash sintered ZnO samples has been conducted and compared to a sample with controlled current ramp (i.e., linear increase of current). It has been found that the rapid densification during flash sintering limits the grain growth leading to finer grain sizes compared to the sample with a controlled current ramp. Stacking faults have been observed in the microstructure of both samples due to the generation of point defects.

Flash sintering has demonstrated the ability to reduce furnace temperatures up to hundreds of degrees below conventional sintering temperature requirements and reduce the dwell time to as low as a few seconds [1]. This technique combines furnace heating and an applied electric field to achieve rapid densification, which occurs during a non-linear rise in current as the sample becomes conductive. Various ceramics have been successfully densified, including yttria-stabilized zirconia (YSZ) [1,2], TiO_2 [3–5], CeO_2 [6], $SrTiO_3$ [7,8], Co_2MnO_4 [9] and composite materials [10,11]. The mechanism(s) of flash sintering of ceramic materials has been extensively studied to understand the non-equilibrium nature during this rapid sintering process, including the implementation of various *in situ* characterization techniques [12,13] and development of multiscale modeling tools [14–16].

ZnO, an intrinsic n-type semiconductor, is one of the well-studied materials in flash sintering besides YSZ [17–25]. Previous studies of flash sintered ZnO have demonstrated that both the applied electrical field and current density significantly influence the grain growth behavior [17]. One of the major challenges of flash sintering is the inhomogeneous microstructure due to non-uniform temperature and defect distribution [18,26,27]. The microstructure of flash sintered ZnO has been shown to be asymmetrical [18] due to different grain growth mechanisms across the samples, including electrochemical and Peltier effects [5,28].

Recently, several studies investigated the mechanisms of flash sintering by comparing with conventional sintering at different temperature ramp rates. Ultra-fast firing demonstrated the ability to increase the rate of sintering by over two orders of magnitude by increasing the heating rate [21,29]. On the other hand, another study compared slow flash sintering with conventional sintering and observed similarities in densification rate and microstructure [7]. Controlling current density ramping rate is a unique approach to control the flash sintering process and investigate the effect of such abrupt increase in current. The current ramp control is performed by gradually increasing the current density limit rather than allowing for the abrupt rise in current density in typical flash sintering experiments.

In this study, a detailed microstructure comparison was performed on the flash sintered ZnO samples, with and without controlled current ramp, to elucidate the effect of the non-linear rise in current on the overall sintering process. A transmission electron microscopy (TEM) study was conducted for both positive and negative electrode regions in these samples with focuses on the grain size distribution, pore morphology and extended defects analysis. Currently there is no prior report on the extended defects in the microstructure of flash sintered ZnO. The microstructure characteristics in flash sintered samples were also compared with the samples sintered without applied field to explore the fundamental flash sintering mechanisms in ZnO.

* Corresponding author at: School of Materials Engineering, Purdue University, West Lafayette, IN 47907, USA.
E-mail address: hwang00@purdue.edu (H. Wang).

https://doi.org/10.1016/j.scriptamat.2018.11.009
1359-6462/

To prepare the green body for flash sintering, ZnO powder (Sigma Aldrich, <100 nm particle size) was uniaxially pressed under 150 MPa load into cylindrical pellets in a stainless steel die. The compacts measured approximately 3 mm in height and 6 mm in diameter, with a green density of 55–60%. The green pellets were loaded into a stage with platinum electrodes attached to the flat faces and heated up to the pre-flash temperature of 700 °C at a heating rate of 10 °C/min. A small pressure of 10 kPa was used to maintain consistent electrical contact between the sample and electrodes. An electric field of 60 V/cm was applied across the sample once the pre-flash temperature was reached. After the onset of flash sintering began, the current density rose until reaching the preset limit of 10 A/cm^2. The power source was switched from voltage control to current control and the current density was held constant for 60 s. Subsequently, the power supply was shut down and the furnace was cooled to room temperature.

For the current ramp sample, a sufficiently higher electric field (120 V/cm) was applied to initiate a sufficiently rapid feedback loop of temperature and conductivity for the current ramp initiate. The power supply was switched into current control mode, where the electric field rapidly dropped to maintain a linear current ramp. A current ramp rate of 0.1 A/cm^2/s was maintained until the current density limit of 10 A/cm^2 was reached, which took approximately 95 s. The current was held at 10 A/cm^2 for 10 s to ensure the electric energy used in both experiments were approximately the same. A sample without an applied field was sintered to 1100 °C at a heating rate of 10 °C/min and held for 60 s before cooling.

Table 1 summarizes the experimental conditions for all the sintered ZnO samples. The final densities were measured using the Archimedes method. The samples were sectioned to prepare plan-view TEM samples, with manual grinding, polishing, dimpling and final polishing in an ion milling system (PIPS II, Gatan). Microstructure characterization was performed using an FEI TALOS 200X TEM operated at 200 kV. The average grain size was measured by direct measurements of 100 grains from multiple TEM images for each sample.

The electric field, current density, power density and linear shrinkage plots for flash sintering and current ramp are shown in Fig. 1. The power density plot shows a power spike reaching ~600 W/cm^3, which is typical for flash sintering and is created during the switch from voltage to current control. The majority of the linear shrinkage for flash sintering occurred during the non-linear increase in the current density as the sample becomes conductive. During the 60 s hold at the current density limit a small linear shrinkage was observed. The small spike in electric field and power density observed around 25 s was due to contact resistance, where the shrinkage resulted in the temporary reduction of contact with the electrodes. Regardless, the electrical field across the sample was sufficient to maintain the desired current during the current control stage. On the other hand, the sample under the controlled current density ramp did not experience a power spike and thus consequently experienced a slower heating rate. The conductivity, however, increased linearly and reached higher values than that of the flash sintered ZnO at the end of 105 s. A gradual increase in linear shrinkage over a 105 s time period occurred rather than an abrupt densification over approximately 6 s for the flash sintered sample. More minor spikes were observed due to a higher probability of contact resistance as a result of continuous changes in sample dimensions during shrinkage.

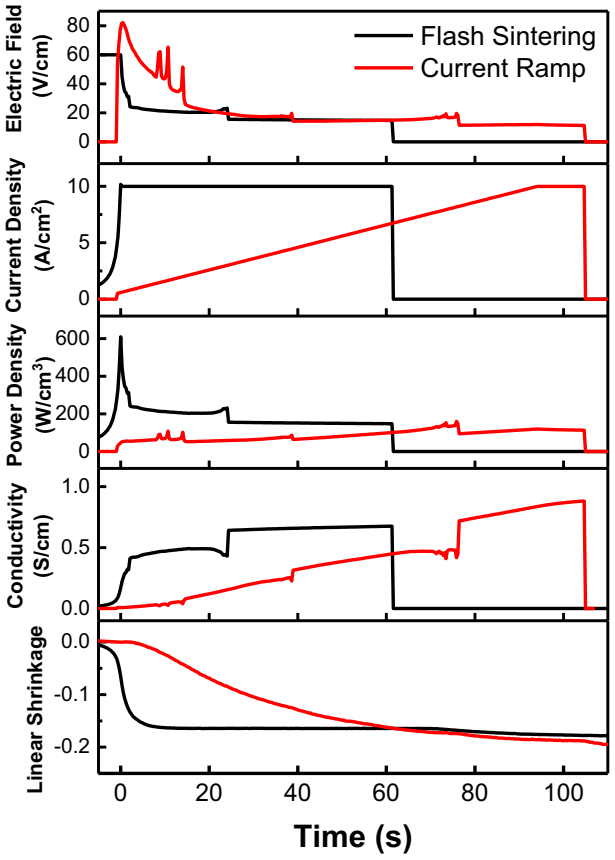

Fig. 1. Plots of electric field, current density, power density, conductivity and linear shrinkage during flash sintering of ZnO with and without a controlled current ramp.

Fig. 2 shows the TEM micrographs of flash sintered and controlled current ramp sintered ZnO at both positive and negative regions with their corresponding diffraction patterns. The average grain size and porosity analyzed from the micrographs are summarized in Table 2. To explore the microstructural differences, the positive and negative regions of both the current ramp and flash sintered samples are shown in Fig. 2. It is notable that both flash sintered and controlled current ramp ZnO did not exhibit obvious differences in grain size between the positive and negative regions. The flash sintered sample had finer grains (average grain size of ~1.3 μm) at both electrodes compared to the current ramp sample (average grain size of ~1.7 μm). This grain size distribution was also confirmed by the diffraction patterns in Fig. 2, where the larger grain size in the current ramp sample produced more distinguished diffraction spots. Another interesting observation is that the flash sintered ZnO had several diffraction spots which are very close together, as marked by the blue circles. The controlled current ramp sample overall had more scattered and distinguished diffraction spots. This suggests that multiple grains with similar orientations exist in the sample in the case of the flash sintered sample.

Table 1
Summary of experimental conditions.

Sample	Furnace temperature (°C)	Initial electric field (V/cm)	Current density limit (A/cm^2)	Current density ramp (A/cm^2/s)	Holding time (s)	Final density
Flash sintering	700	60	10	–	60	95%
Current ramp	700	120	10	0.1	10	95%
No applied field	1100	–	–	–	60	94%

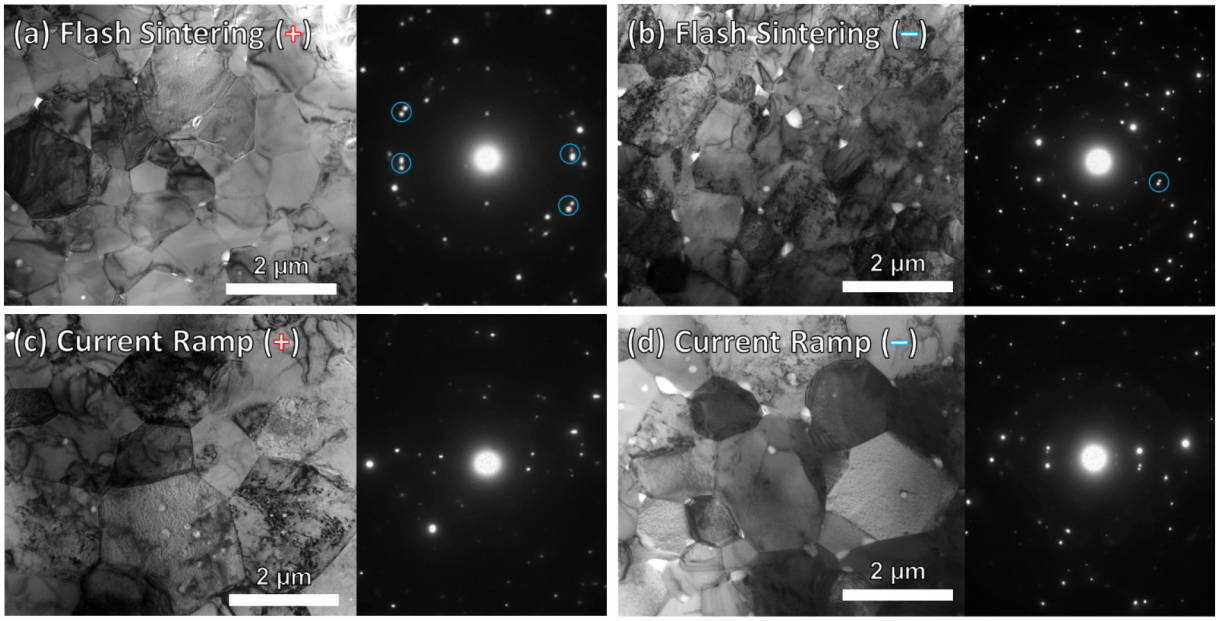

Fig. 2. TEM micrographs of ZnO after (a)-(b) flash sintering and (c)-(d) current ramp at the positive and negative ends respectively, with their corresponding diffraction patterns. The blue circles mark diffraction spots which are very close together, suggesting subgrain texturing. (For interpretation of the references to colour in this figure legend, the reader is referred to the web version of this article.)

Although there was no obvious difference in grain size between the two electrode regions, the pore content and distribution are quite different for the two electrode regions. Specifically, the amount of porosity was found to be much higher in the negative region than the positive region for both flash sintering and current ramp samples. Additionally, the pore morphology is quite different between the two samples and the two electrode regions. Fig. 3 compares the microstructure at a higher magnification for a clear comparison of the intergranular porosity (i.e., pores between grains or at triple junctions) and intragranular porosity (i.e., pores within grains). The positive region of the flash sintered ZnO, as shown in Fig. 3 (a), has very low porosity (0.3%), mostly consisting of intergranular porosity and very few intragranular pores. On the negative electrode region, there is approximately 1.1% of porosity, which is also predominantly intergranular porosity with some intragranular porosity. The current ramp sample demonstrated a similar porosity difference in the positive and negative regions. However, there were many more intragranular pores, especially at the positive electrode region, as illustrated in Fig. 3 (c) where many entrapped pores have been observed in a single grain. The negative electrode region of the current ramp sample (Fig. 3 (d)) had an equal distribution of intergranular and intragranular porosity.

The comparison of the flash sintering and current ramp ZnO samples at the isothermal furnace temperature shows clear differences in grain size and pore morphology. Although using a controlled current ramp did not experience as high as the maximum power dissipation of the flash sintered sample, it has led to larger grain sizes. Based on sample temperature estimations using the blackbody radiation (BBR) model and *in situ* XRD lattice expansion, as shown in the supplementary, the sample temperature achieved by the flash sintered ZnO should be higher due to the higher power dissipation. Hence, the observed microstructural differences can be attributed to the rate of heating experienced by the samples. The power spike in flash sintering allows for a more rapid heating of the sample, and hence accelerating the densification process over grain growth. A clear indication of rapid heating is the limited grain coarsening and the small concentration of intergranular pores. Additionally, during the steady state of the current holding period, the intergranular pores cause pore drag which limits the grain growth and produces a finer grain structure for the flash sintered ZnO. The intragranular porosity found in the controlled current ramp is an indication of pore breakaway during grain growth as the boundary migration velocity exceeds the pore migration velocity [30]. This is typically observed when the pore mobility increases as the pore shrinks due to densification. The gradual densification process in the current ramp increases the probability of pores separating from the boundaries, leading to high intragranular porosity. Once the pores are separated, grain growth can occur more easily, which further supports the observation of the larger average grain size in the current ramp ZnO.

In a prior study on flash sintered ZnO, asymmetric grain sizes between the electrodes were reported due to potential induced abnormal grain growth at the anode [18]. This study could not demonstrate such difference in grain size since the electric field used was significantly lower. Nonetheless, the difference in pore content between the electrodes clearly suggests a dissimilar densification rate. Similar temperature gradients have been observed in flash sintered TiO_2, which is another n-type semiconductor, based on in situ EDXRD study [31]. This was attributed to the Peltier effect, where an electric current passing through a junction leads to heating and cooling effects. Based on the porosity difference between electrodes for both with and without controlled current ramp, the Peltier effect could be responsible for the difference in densification rate at the positive and negative electrodes.

Fig. 4 (a) and (b) shows the TEM images of the flash sintered and current ramp ZnO samples compared with a conventional sintered ZnO without applied electrical field (Fig. 4 (c)). High density stacking faults which are representative characteristics of the flash sintered and current ramp ZnO. The stacking faults shown here are from the positive

Table 2
Final density, grain size and porosity of ZnO after flash sintering and current ramp sintering. The grain size and porosity were measured from TEM micrographs.

Sample	Grain size (μm)		Porosity (%)	
	+	−	+	−
Flash sintering	1.3 ± 0.3	1.2 ± 0.2	0.34	1.10
Current ramp	1.7 ± 0.3	1.6 ± 0.3	0.21	0.99

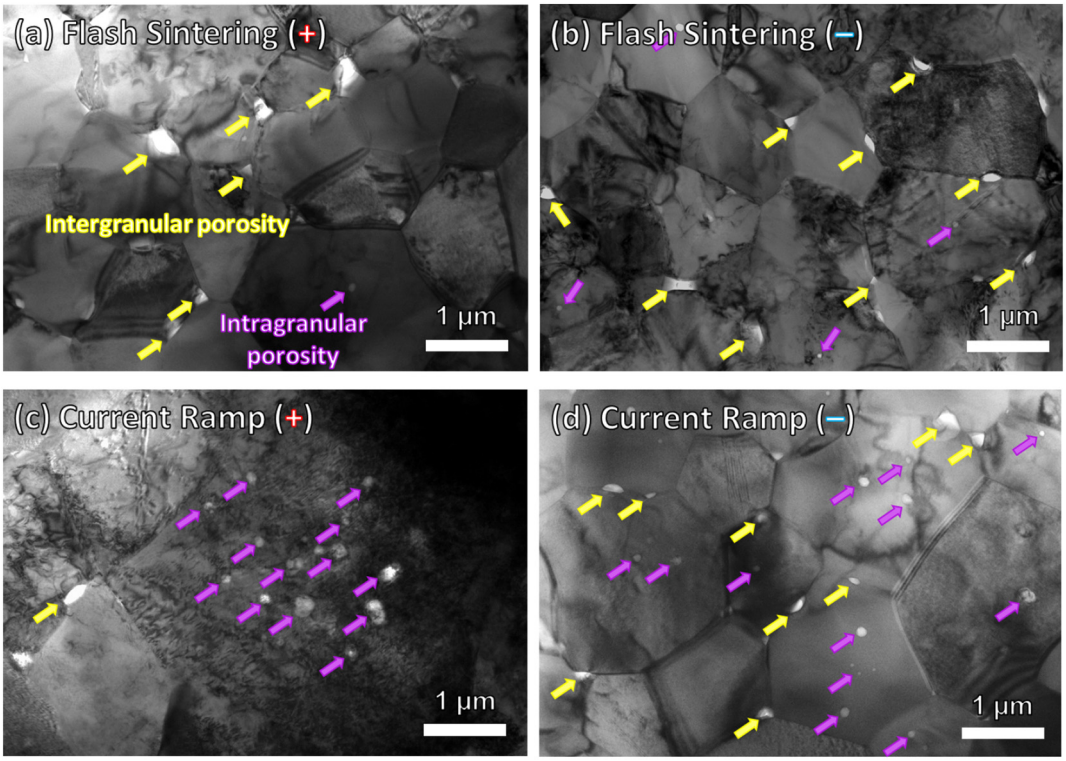

Fig. 3. Difference in pore morphology in ZnO after (a)-(b) flash sintering and (c)-(d) current ramp at the positive and negative ends respectively. The yellow arrows mark intergranular pores and the purple arrows mark intragranular pores. (For interpretation of the references to colour in this figure legend, the reader is referred to the web version of this article.)

electrode region. The negative regions in both flash sintered and current ramp samples (not shown here) also show obvious stacking faults. Stacking faults are planar defects caused by changes of atomic plane stacking sequence and are found in multiple grains for the flash sintered sample, as marked by the orange arrows in Fig. 4 (a). These stacking faults exist across the grains, i.e., begin and terminate at grain boundaries of a single grain. The current ramp ZnO also demonstrated multiple stacking faults in a grain, as shown in Fig. 4 (b), along with bands made up of short stacking fault segments going across the grain. To identify if the presence of extended planar defects was due to an applied field, the microstructure of a ZnO sample sintered without any applied field was compared. The sintering temperature selected was higher than the flash sintering ones, since a previous in situ energy dispersive X-ray diffraction (EDXRD) predicted the temperature at 10 A/cm^2 to be approximately 1100 °C during flash sintering [25]. The microstructure, as shown in Fig. 4 (c), illustrates reasonable densification without any apparent extended defects. It may be possible that defects can be annihilated due to more intensive grain growth which occurred in the sintered sample without field (average grain size ~3.1 μm). However, high density stacking faults remained even after significant grain growth in flash sintered titania [32], which confirms the formation of stacking faults due to the applied field.

The flash sintered ZnO samples show microstructural similarities and differences compared to flash sintered YSZ ones. The diffraction pattern of flash sintered ZnO demonstrated clustered diffraction spots, i.e., several diffraction spots are very close to each other (Fig. 2), indicating possible texturing of subgrains. A similar local texturing phenomenon has been reported in flash sintered YSZ [33]. Based on the electron diffraction data, there is a stronger texture in the positive electrode region of the flash sintered ZnO compared to the negative side, which may suggest the involvement of additional mechanisms at the positive side to assist in the densification process. The diffraction patterns of the current ramp ZnO did not show obvious texturing structure, which may imply the texturing phenomena are more pronounced in the flash sintering process.

Another difference in the features of ZnO compared to YSZ is the type of extended defects observed. Dislocation arrays were observed in the flash sintered YSZ microstructure [33,34], rather than stacking faults as shown for the case of ZnO. In ZnO thin films, the basal-plane stacking faults (i.e., (0001) plane stacking) are known to have very low formation energies [35]. As a result, high density of stacking faults can be formed in ZnO thin films due to high point defect concentrations and consequently affect the overall electrical conductivity in ZnO [36]. A depth-resolved cathodoluminescence experiment on flash sintered ZnO has also demonstrated a higher increase in native point defects concentration within the grains compared to the grain boundaries after flash sintering [20]. This is expected as grain boundaries act as sinks for oxygen vacancies. Hence, extended defects such as stacking faults exist in the flash sintered and controlled current ramp samples due to an increase in the density of point defects and electrical conductivity introduced by the applied electrical field.

Evidently, the microstructure of ZnO sintered without any applied field did not reveal any extended defects compared to the flash sintered or controlled current ramp samples. In addition, the controlled current ramp sample also contained bands of short segments of stacking faults, which could be a consequence of the gradual increase in conductivity over a longer time during the current ramping process. Overall, the extended defects generated during the flash sintering process appear to be dependent on the nature of the materials and the defect formation energy for the materials. Further investigation of the types of extended defects present in other flash sintered ceramics under different sintering conditions and stages are critical for the study of fundamental mechanisms related to field assisted sintering.

In summary, the microstructure of flash sintered ZnO samples, with and without controlled current ramp were investigated and compared. Flash sintered ZnO produced fine grains by minimizing grain growth

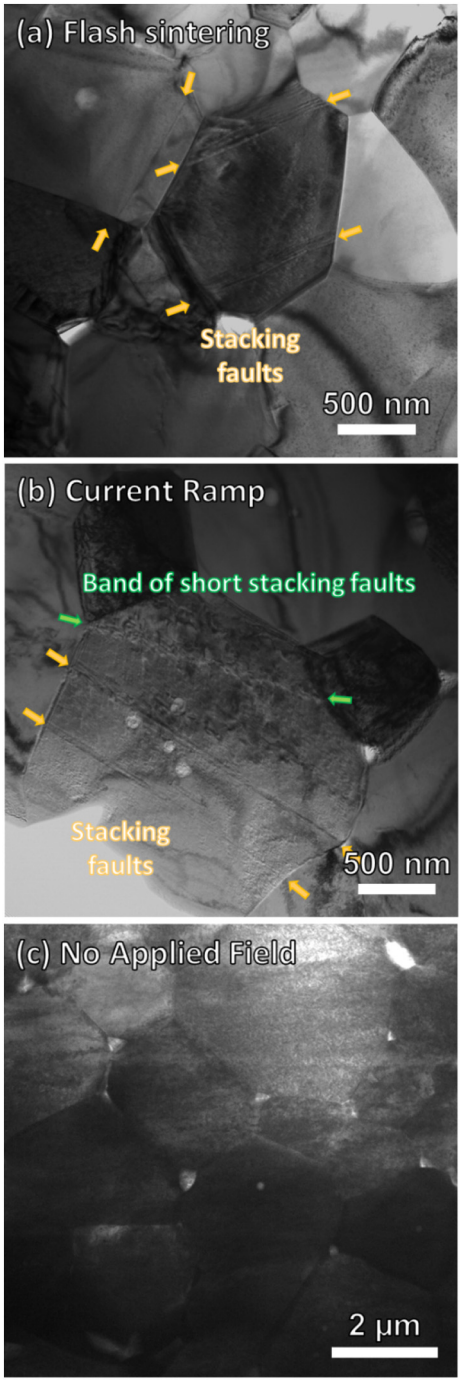

Fig. 4. Representative micrographs of the extended defects present in the (a) flash sintered and (b) current ramp ZnO. The orange arrows indicate stacking faults while the green arrows mark a band of short stacking faults. (c) The microstructure of ZnO sintered without an applied field is poorly sintered with a larger grain size and does not contain any extended defects. (For interpretation of the references to colour in this figure legend, the reader is referred to the web version of this article.)

due to rapid densification during the non-linear increase in current. A controlled current ramp leads to gradual densification, resulting in larger grains with mostly intragranular porosity. Consequently, more pores break away from the grain boundaries and accelerate grain growth. This comparison study signifies the importance of the non-linear rise in current in order to achieve high density with fine gain structures. The applied field leads to the formation of stacking faults in both flash sintered and current ramp ZnO due to the generation of point defects during the field-assisted process.

Acknowledgements

We would like to acknowledge the support from the U.S. Office of Naval Research (Contract number: N00014-17-1-2087 for sintering effort and N00014-16-1-2778 for TEM). The effort at Rutgers University was supported by the U.S. Office of Naval Research (Contract number: N00014-15-1-2492).

Appendix A. Supplementary data

Supplementary data to this article can be found online at https://doi.org/10.1016/j.scriptamat.2018.11.009.

References

[1] M. Cologna, B. Rashkova, R. Raj, J. Am. Ceram. Soc. 93 (2010) 3556.
[2] M. Cologna, A.L. Prette, R. Raj, J. Am. Ceram. Soc. 94 (2011) 316.
[3] S.K. Jha, R. Raj, J. Am. Ceram. Soc. 97 (2014) 527.
[4] S.K. Jha, J.M. Lebrun, K.C. Seymour, W.M. Kriven, R. Raj, J. Eur. Ceram. Soc. 36 (2016) 257.
[5] H. Charalambous, S.K. Jha, H. Wang, X.L. Phuah, H. Wang, T. Tsakalakos, Scr. Mater. 155 (2018) 37.
[6] S.K. Jha, H. Charalambous, H. Wang, X.L. Phuah, C. Mead, J. Okasinski, H. Wang, T. Tsakalakos, Ceram. Int. 44 (2018) 15362.
[7] F. Lemke, W. Rheinheimer, M.J. Hoffmann, Scr. Mater. 130 (2017) 187.
[8] A. Karakuscu, M. Cologna, D. Yarotski, J. Won, J.S. Francis, R. Raj, B.P. Uberuaga, J. Am. Ceram. Soc. 95 (2012) 2531.
[9] A.L. Prette, M. Cologna, V. Sglavo, R. Raj, J. Power Sources 196 (2011) 2061.
[10] E. Bichaud, J.M. Chaix, C. Carry, M. Kleitz, M.C. Steil, J. Eur. Ceram. Soc. 35 (2015) 2587.
[11] A. Gaur, V.M. Sglavo, J. Am. Ceram. Soc. 98 (2015) 1747.
[12] S.K. Jha, X.L. Phuah, J. Luo, C.P. Grigoropoulos, H. Wang, R.E. García, B. Reeja-Jayan, J. Am. Ceram. Soc. 102 (2018) 5.
[13] K. Terauds, J.M. Lebrun, H.H. Lee, T.Y. Jeon, S.H. Lee, J.H. Je, R. Raj, J. Eur. Ceram. Soc. 35 (2015) 3195.
[14] R.I. Todd, E. Zapata-Solvas, R.S. Bonilla, T. Sneddon, P.R. Wilshaw, J. Eur. Ceram. Soc. 35 (2015) 1865.
[15] J. Narayan, Scr. Mater. 68 (2013) 785.
[16] S. Grasso, Y. Sakka, N. Rendtorff, C. Hu, G. Maizza, H. Borodianska, O. Vasylkiv, J. Ceram. Soc. Jpn. 119 (2011) 144.
[17] C. Schmerbauch, J. Gonzalez-Julian, R. Röder, C. Ronning, O. Guillon, J. Am. Ceram. Soc. 97 (2014) 1728.
[18] Y. Zhang, J.I. Jung, J. Luo, Acta Mater. 94 (2015) 87.
[19] Y. Zhang, J. Luo, Scr. Mater. 106 (2015) 26.
[20] H. Gao, T.J. Asel, J.W. Cox, Y. Zhang, J. Luo, L.J. Brillson, J. Appl. Phys. 120 (2016) 105302.
[21] Y. Zhang, J. Nie, J.M. Chan, J. Luo, Acta Mater. 125 (2017) 465.
[22] J. Nie, Y. Zhang, J.M. Chan, S. Jiang, R. Huang, J. Luo, Scr. Mater. 141 (2017) 6.
[23] J. Luo, Scr. Mater. 146 (2018) 260.
[24] H. Charalambous, S.K. Jha, K.H. Christian, T. Tsakalakos, J. Eur. Ceram. Soc. 38 (2018) 3689.
[25] H. Charalambous, S.K. Jha, R. Lay, A. Cabales, J. Okasinski, T. Tsakalakos, Ceram. Int. 44 (2018) 6162.
[26] S.W. Kim, S.G. Kim, J.I. Jung, S.J.L. Kang, I.W. Chen, J. Am. Ceram. Soc. 94 (2011) 4231.
[27] R. Muccillo, E.N.S. Muccillo, J. Eur. Ceram. Soc. 34 (2014) 915.
[28] M. Yu, S. Grasso, R. Mckinnon, T. Saunders, M.J. Reece, Adv. Appl. Ceram. 116 (2017) 24.
[29] W. Ji, B. Parker, S. Falco, J.Y. Zhang, Z.Y. Fu, R.I. Todd, J. Eur. Ceram. Soc. 37 (2017) 2547.
[30] S. J. L. Kang (2004). Butterworth-Heinemann.
[31] H. Charalambous, S.K. Jha, X.L. Phuah, H. Wang, H. Wang, J. Okasinski, T. Tsakalakos, J. Eur. Ceram. 38 (2018) 5503.
[32] H. Wang, X. L. Phuah, H. Charalambous, S. K. Jha, J. Li, T. Tsakalakos, X. Zhang, H. Wang. (2018) (in preparation).
[33] H. Wang, X.L. Phuah, J. Li, T.B. Holland, K.S.N. Vikrant, Q. Li, S. Hellberg, N. Bernstein, R.E. García, A.K. Mukherjee, X. Zhang, H. Wang, Ceram. Int. 45 (2018) 1251.
[34] J. Cho, Q. Li, H. Wang, Z. Fan, J. Li, S. Xue, S. Karra, H. Wang, T.B. Holland, A.K. Mukherjee, R.E. García, X. Zhang, Nat. Commun. 9 (2018) 2063.
[35] M. Schirra, R. Schneider, A. Reiser, G.M. Prinz, M. Feneberg, J. Biskupek, U. Kaiser, C.E. Krill, K. Thonke, R. Sauer, Phys. Rev. B 77 (2008), 125215. .
[36] D. Gerthsen, D. Litvinov, T. Gruber, C. Kirchner, A. Waag, Appl. Phys. Lett. 81 (2002) 3972.